

# How volumetric-deviatoric coupling influences the crack prediction in concrete fracture tests

R. Rempling

*Chalmers University of Technology, Gothenburg, Sweden*

P. Grassl

*University of Glasgow, Glasgow, Scotland, United Kingdom*

**ABSTRACT:** The present paper analyzes the influence of volumetric-deviatoric coupling on the prediction of curved crack patterns in concrete fracture tests. The influence is analyzed by an elasto-plastic-damage model and the coupling is controlled by the hardening modulus of the plasticity model. First, the tangent stiffness matrix and the total stress-strain response for simple shear are investigated. Then, two fracture tests reported in the literature are simulated with significantly varying amounts of coupling. It is shown that volumetric-deviatoric coupling greatly improves the description of curved crack patterns in mixed-mode fracture tests.

## 1 INTRODUCTION

Constitutive models based on damage mechanics, plasticity and combinations of both are often used to describe the fracture process of quasi-brittle materials, such as concrete, rock, tough ceramics or ice. In these materials, fracture is characterized by the development of nonlinear fracture process zones, which can be described macroscopically as regions of highly localized strains. The performance of constitutive models for concrete is often evaluated by analyzing fracture tests with curved crack patterns Arrea and Ingraffea (1982), Nooru-Mohamed (1992), Schlangen (1993), Galvez et al. (1998). The results of such analysis have been reported by Cendón et al. (2000), di Prisco et al. (2000), Geers et al. (2000), Grassl and Jirásek (2004), Ožbolt and Reinhardt (2002), Patzák and Jirásek (2003), Pivonka et al. (2004). Anisotropic damage models have proved to be capable of reproducing many of the often complex crack patterns, as reported by Patzák and Jirásek (2003). Isotropic damage models, on the contrary, often fail to describe realistically the crack patterns of these mixed-mode fracture tests. Anisotropic damage models differ from isotropic ones in, among other things, that they provide volumetric-deviatoric coupling, i.e. in a simple shear test, the shear strain generates not only a shear stress, but also compressive normal stresses. Simple shear is defined as a state with three-dimensional constant volume strain. Willam et al. (2001) have studied the volumetric-deviatoric coupling on the constitutive level for various plasticity models with regard to loss of stability and uniqueness.

The present paper investigates the influence of volumetric-deviatoric coupling on the modeling of

mixed mode fracture tests. This is accomplished by using an isotropic elasto-plastic-damage model for which the hardening law of the plasticity model is controlled. Controlling the hardening law makes it possible to vary the amount of volumetric-deviatoric interaction. It is expected that this interaction is the key to an accurate description of curved crack patterns observed in several fracture tests of plain concrete. This has not been shown before to the knowledge of the authors. Thus, this study contains novel features, which help to understand the performance of modeling techniques for concrete subjected to complex combinations of loading.

The assumption of plane stress is often used for analyzing the mentioned fracture tests. Consequently, a modified simple shear state is examined, where the condition of constant volume strain is limited to the in-plane strain components, and the out-of-plane component is determined from the condition of zero stress in this direction.

The basic equations of the elasto-plastic-damage model are stated and the volumetric-deviatoric interaction is illustrated with the elasto-plastic-damage tangent stiffness matrix for the onset of inelastic behavior in simple shear. Next, the total stress-strain response for this state is analyzed with the model for four different degrees of interaction. Finally, two fracture tests with curved crack patterns, reported in the literature, are analyzed with significantly varying amounts of volumetric-deviatoric coupling.

## 2 THE PLASTICITY-DAMAGE MODEL

The model consists of an elasto-plasticity part combined with isotropic damage that is determined by the cumulative plastic strain. For the combined elasto-plastic-damage model, the stress-strain relation is given as

$$\boldsymbol{\sigma} = (1 - \omega) \bar{\boldsymbol{\sigma}} = (1 - \omega) \mathbf{D}_e : (\boldsymbol{\varepsilon} - \boldsymbol{\varepsilon}_p) \quad (1)$$

where  $\boldsymbol{\sigma}$  is the nominal stress,  $\omega$  is the scalar describing the amount of isotropic damage,  $\bar{\boldsymbol{\sigma}}$  is the effective stress,  $\mathbf{D}_e$  is the isotropic elastic stiffness,  $\boldsymbol{\varepsilon}$  is the total strain and  $\boldsymbol{\varepsilon}_p$  is the plastic strain.

### 2.1 Basic equations

The plasticity model, which is formulated on the assumption of small strains, is based on the effective stress,  $\bar{\boldsymbol{\sigma}}$ , and consists of the yield function, the flow rule, the evolution law for the hardening variable and the loading-unloading conditions. For plane stress

$$f_p(\bar{\boldsymbol{\sigma}}, \kappa_p) = \bar{\sigma}_1 - \sigma_y(\kappa_p) = \bar{\sigma}_1 - (f_t + H_p \kappa_p) \quad (2)$$

describes the Rankine yield function, where  $\bar{\sigma}_1$  is the maximum principal value of the effective stress tensor  $\bar{\boldsymbol{\sigma}}$ ,  $\sigma_y$  is the yield stress,  $f_t$  is the tensile strength,  $H_p$  is the plastic hardening modulus and  $\kappa_p$  is the plastic hardening parameter. Plastic yielding is initiated when the maximum principal effective stress reaches the yield stress  $\sigma_y$ . For equibiaxial tension, when both principal values are equal to the yield stress, the value of the second principal stress also influences the yielding process. Only one active surface is dealt with here, since the behavior is studied in biaxial tension and compression, see Figure 1a. For the structural analysis in Section 4, however, the case of two active yield surfaces for equibiaxial tension is included. For one active surface, the flow rule is given as

$$\dot{\boldsymbol{\varepsilon}}_p = \dot{\lambda} \frac{\partial f_p}{\partial \bar{\boldsymbol{\sigma}}} = \dot{\lambda} \frac{\partial \bar{\sigma}_1}{\partial \bar{\boldsymbol{\sigma}}} = \dot{\lambda} \mathbf{n}_1 \otimes \mathbf{n}_1 \quad (3)$$

where  $\mathbf{n}_1$  is the normalized eigenvector corresponding to the first principal eigenvalue of the effective stress tensor,  $\otimes$  denotes the dyadic product of two vectors, and  $\dot{\lambda}$  is the rate of the plastic multiplier. The evolution of the hardening parameter,  $\kappa_p$ , is given by the norm of the plastic strain rate

$$\dot{\kappa}_p = \|\dot{\boldsymbol{\varepsilon}}_p\| = \dot{\lambda} \quad (4)$$

Loading-unloading conditions complete the description of the plasticity part:

$$f_p \leq 0 \quad \dot{\lambda} \geq 0 \quad \dot{\lambda} f_p = 0 \quad (5)$$

The damage variable,  $\omega$ , is related to the plastic hardening parameter,  $\kappa_p$ , by

$$\omega = g_d(\kappa_p) = 1 - \frac{f_t \exp(-\kappa_p/\varepsilon_f)}{f_t + \kappa_p H_p} \quad (6)$$

which results in an exponential total stress-strain curve, see Figure 1b. The model parameter,  $\varepsilon_f$ , controls the area under the stress strain curve and can be related to the fracture energy  $G_F$ . There is no plastic process without damage evolution, since it is directly linked to the plastic process.

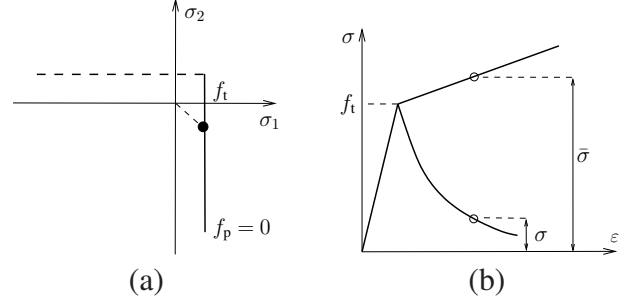


Figure 1: (a) Schematic drawing of the Rankine yield surface at the onset of yielding for pure shear. (b) Schematic drawing of the stress-strain and effective stress-strain curve for uniaxial tension.

### 2.2 The tangent stiffness matrix

The tangent stiffness is studied to gain information on the form of the volumetric-deviatoric coupling, which is introduced by the plastic-damage model. The rate form of the general stress-strain relation in Eq. (1) is

$$\begin{aligned} \dot{\boldsymbol{\sigma}} &= (1 - \omega) \dot{\bar{\boldsymbol{\sigma}}} - \dot{\omega} \bar{\boldsymbol{\sigma}} = \\ &(1 - \omega) \mathbf{D}_e : \left( \dot{\boldsymbol{\varepsilon}} - \dot{\lambda} \frac{\partial \bar{\sigma}_1}{\partial \bar{\boldsymbol{\sigma}}} \right) - g'_d \dot{\lambda} \mathbf{D}_e : (\boldsymbol{\varepsilon} - \boldsymbol{\varepsilon}_p) \end{aligned} \quad (7)$$

where

$$\begin{aligned} g'_d &= \frac{\partial g_d}{\partial \kappa_p} = \frac{f_t/\varepsilon_f \exp(-\kappa_p/\varepsilon_f) (f_t + \kappa_p H_p)}{(f_t + \kappa_p H_p)^2} \\ &+ \frac{f_t \exp(-\kappa_p/\varepsilon_f) H_p}{(f_t + \kappa_p H_p)^2} \end{aligned} \quad (8)$$

The plastic multiplier,  $\dot{\lambda}$ , is determined from the consistency condition of the plasticity part

$$\dot{f}_p = \frac{\partial \bar{\sigma}_1}{\partial \bar{\boldsymbol{\sigma}}} \mathbf{D}_e : \left( \dot{\boldsymbol{\varepsilon}} - \dot{\lambda} \frac{\partial \bar{\sigma}_1}{\partial \bar{\boldsymbol{\sigma}}} \right) - \dot{\lambda} H_p = 0 \quad (9)$$

as

$$\dot{\lambda} = \frac{\frac{\partial \bar{\sigma}_1}{\partial \bar{\boldsymbol{\sigma}}} : \mathbf{D}_e : \dot{\boldsymbol{\varepsilon}}}{\frac{\partial \bar{\sigma}_1}{\partial \bar{\boldsymbol{\sigma}}} : \mathbf{D}_e : \frac{\partial \bar{\sigma}_1}{\partial \bar{\boldsymbol{\sigma}}} + H_p} \quad (10)$$

By setting Eq. (10) in Eq. (7)

$$\dot{\boldsymbol{\sigma}} = \mathbf{D}_{epd} : \dot{\boldsymbol{\varepsilon}} \quad (11)$$

is obtained, where

$$\mathbf{D}_{\text{epd}} = (1 - \omega) \left( \mathbf{D}_e - \frac{\mathbf{D}_e : \frac{\partial \bar{\sigma}_1}{\partial \bar{\boldsymbol{\sigma}}} \otimes \frac{\partial \bar{\sigma}_1}{\partial \bar{\boldsymbol{\sigma}}} : \mathbf{D}_e}{\frac{\partial \bar{\sigma}_1}{\partial \bar{\boldsymbol{\sigma}}} : \mathbf{D}_e : \frac{\partial \bar{\sigma}_1}{\partial \bar{\boldsymbol{\sigma}}} + H_p} \right) - g'_d \left( \frac{\mathbf{D}_e : (\boldsymbol{\varepsilon} - \boldsymbol{\varepsilon}_p) \otimes \frac{\partial \bar{\sigma}_1}{\partial \bar{\boldsymbol{\sigma}}} : \mathbf{D}_e}{\frac{\partial \bar{\sigma}_1}{\partial \bar{\boldsymbol{\sigma}}} : \mathbf{D}_e : \frac{\partial \bar{\sigma}_1}{\partial \bar{\boldsymbol{\sigma}}} + H_p} \right) \quad (12)$$

is the tangent stiffness of the elasto-plastic-damage model for one active surface.

Now, the tangent stiffness for simple shear is analyzed. Before the onset of inelastic behavior the stress state in simple shear is determined by the isotropic elastic stiffness matrix as

$$\begin{Bmatrix} 0 \\ 0 \\ \sigma_{12} \end{Bmatrix} = \frac{E}{1 - \nu^2} \begin{bmatrix} 1 & \nu & 0 \\ \nu & 1 & 0 \\ 0 & 0 & \frac{1 - \nu}{2} \end{bmatrix} \begin{Bmatrix} 0 \\ 0 \\ \gamma_{12} \end{Bmatrix} \quad (13)$$

where  $E$  is Young's modulus and  $\nu$  is Poisson's ratio. The shear strain rate results in a shear stress rate only, since the components (1, 3) and (2, 3) of the isotropic linear elastic stiffness matrix in Eq. (13) are equal to zero. Thus, for isotropic elasticity, simple shear coincides with pure shear since the normal strain and stress components are zero. The direction of the maximum principal stress component with respect to the Cartesian coordinate system, for this stress state, is determined as

$$\mathbf{n}_1 = \{1/\sqrt{2} \quad 1/\sqrt{2}\}^T \quad (14)$$

Now, Eq. (3) is used to determine the derivative of the maximum principal stress, with respect to the effective stress tensor, which results in engineering notation to

$$\frac{\partial \bar{\sigma}_1}{\partial \bar{\boldsymbol{\sigma}}} = \{1/2 \quad 1/2 \quad 1\}^T \quad (15)$$

Finally, we set Eq. (15) and Eq. (8) into (12) and obtain, for the onset of the inelastic behavior ( $\kappa_p = \omega = 0$ ,  $\boldsymbol{\varepsilon}_p = \mathbf{0}$  and  $\sigma_{12} = f_t$ )

$$\mathbf{D}_{\text{epd}} = \mathbf{D}_e - \mathbf{R}_p - \mathbf{R}_d \quad (16)$$

where  $\mathbf{D}_e$  is the elastic stiffness matrix in Eq. (13),  $\mathbf{R}_p$  is the contribution of the plasticity part with

$$\mathbf{R}_p = \frac{1}{h_p} \frac{E^2}{4(1 - \nu^2)^2} \begin{bmatrix} (1 + \nu)^2 & (1 + \nu)^2 & 1 - \nu^2 \\ (1 + \nu)^2 & (1 + \nu)^2 & 1 - \nu^2 \\ 1 - \nu^2 & 1 - \nu^2 & (1 - \nu)^2 \end{bmatrix} \quad (17)$$

and  $\mathbf{R}_d$  is the contribution of the damage part with

$$\mathbf{R}_d = \frac{g'_d}{h_p} \frac{E}{2(1 - \nu^2)} \begin{bmatrix} 0 & 0 & 0 \\ 0 & 0 & 0 \\ f_t(1 + \nu) & f_t(1 + \nu) & f_t(1 - \nu) \end{bmatrix} \quad (18)$$

Furthermore,

$$h_p = \frac{E(5 + 3\nu)}{8(1 - \nu^2)} + H_p \quad (19)$$

and

$$g'_d = \frac{1}{\varepsilon_f} + \frac{H_p}{f_t} \quad (20)$$

The matrix,  $\mathbf{R}_p$ , provides volumetric-deviatoric coupling, since the components (1, 3) and (2, 3) of  $\mathbf{R}_p$  are not zero for finite values of  $H_p$ . A shear strain rate,  $\dot{\gamma}_{12}$ , results, therefore, not only in a shear stress rate  $\dot{\sigma}_{12}$ , but also in two normal stress rates,  $\dot{\sigma}_{11} = \dot{\sigma}_{22}$ . The components (1, 3) and (2, 3) of  $\mathbf{R}_d$ , on the other hand, are zero, so that the damage part does not provide any volumetric-deviatoric coupling. The value of  $h_p$  in Eq. (19) depends on the hardening modulus,  $H_p$ . Consequently, the amount of volumetric-deviatoric coupling given by  $\mathbf{R}_p$  is controlled by  $H_p$ . For the limit  $H_p = \infty$ , the components of  $\mathbf{R}_p$  are zero and the volumetric-deviatoric coupling vanishes. The components of matrix  $\mathbf{R}_d$ , however, do not tend to zero for  $H_p \rightarrow \infty$ , since  $g'_d$  in Eq. (20) depends also on  $H_p$ , so that

$$\lim_{H_p \rightarrow \infty} \left( \frac{g'_d}{h_p} \right) = \frac{1}{f_t} \quad (21)$$

Thus, the elasto-plastic-damage stiffness is reduced to a pure elasto-damage stiffness for  $H_p \rightarrow \infty$ .

### 3 ELASTO-PLASTIC DAMAGE SIMULATION OF A SIMPLE SHEAR TEST IN PLANE STRESS

The total stress-strain response of the damage-plasticity model was analyzed, in particular the influence of volumetric-deviatoric interaction on the simple shear response. Four values of the plastic hardening modulus,  $H_p$ , ranging from 0 to  $100E$  are used. The other model parameters chosen are  $E = 30$  GPa,  $\nu = 0.18$ ,  $f_t = 3.5$  MPa and  $\varepsilon_f = 0.0004$ .

The influence of  $H_p$  is illustrated by the unloading behavior in uniaxial tension in Figure 2. For  $H_p = 0$ , the inelastic strain is mainly irreversible ( $\boldsymbol{\varepsilon}_p - \omega \boldsymbol{\varepsilon}_p$ ), while only a small amount of inelastic strain is reversible ( $\omega \boldsymbol{\varepsilon}$ ).

The situation is different for  $H_p = 100E$ , where the plastic strain is nearly zero and the inelastic strains are almost fully reversible. Thus, the model unloads

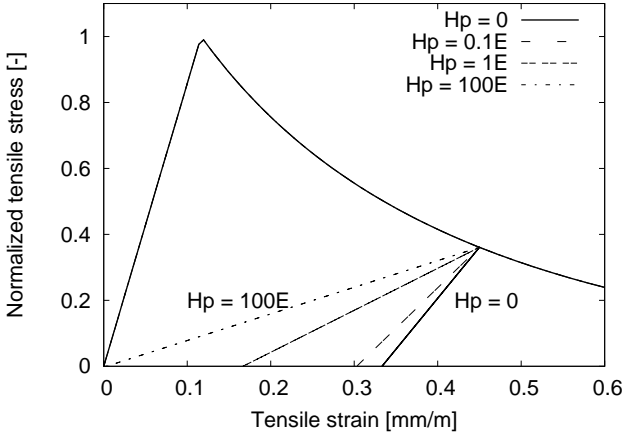


Figure 2: The influence of the plastic hardening modulus  $H_p$  on the unloading stiffness for the elasto-plastic-damage Rankine model. The tensile stress is normalized by the tensile strength  $f_t$ .

almost back to the origin of the stress-strain curve in the figure.

Also, the amount of volumetric-deviatoric coupling differs. This is illustrated by a simple shear test in plane stress. In this strain controlled test, the shear strain is increased, while the two normal strain components are kept at zero. The shear stress-strain response is strongly influenced by the value of the plastic hardening modulus,  $H_p$ , which controls the amount of volumetric-deviatoric interaction, see Figure 3. The maximum shear stress for  $H_p = 0$

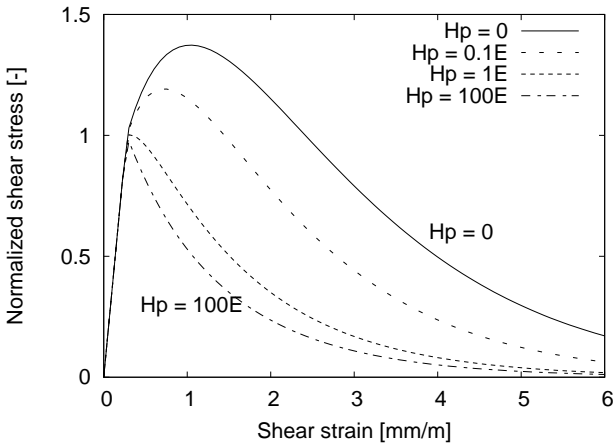


Figure 3: The influence of the plastic hardening modulus,  $H_p$ , on the response in simple shear for the elasto-plastic-damage Rankine model. The shear stress is normalized by the tensile strength  $f_t$

(strong interaction) is nearly 1.4 times greater than for  $H_p = 100E$  (weak interaction). This difference is explained by the activation of normal compressive stresses when there is volumetric-deviatoric interaction, see Figure 4. When the plasticity model has a strong influence, normal plastic strain components develop; since the total strain in the normal direction is fixed, these lead to normal compressive stresses. For  $H_p = 100E$  (weak influence) almost no normal compressive stresses are activated.

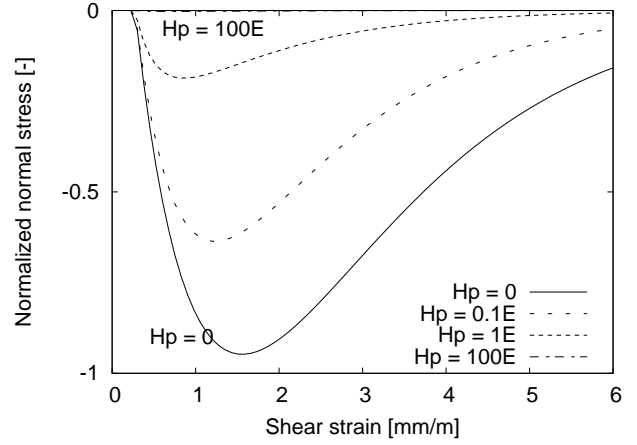


Figure 4: The amount of activated negative normal stress due to the volumetric-deviatoric interaction, which is controlled by the plastic hardening modulus,  $H_p$ . The normal stress is normalized by the tensile strength,  $f_t$ .

It should be stressed that the volumetric-deviatoric coupling not only depends on the hardening modulus, which in the present study controls the ratio of damage and plasticity, but also on the form of the yield surface and flow rule of the plasticity model. However, in the present study only a Rankine plasticity model is considered for simplicity and coupling is only controlled by the hardening modulus.

#### 4 ANALYSIS OF FRACTURE TESTS

In the present section the results of finite element simulations of two fracture tests with curved crack patterns are presented. The crack band approach, Bažant and Oh (1983), is used to obtain a mesh independent description of the dissipated energy. Two amounts of volumetric-deviatoric coupling,  $H_p = 0$  and  $H_p = 100E$ , are considered. The plastic hardening modulus of  $H_p = 0$  corresponds to strong coupling, while  $H_p = 100E$  corresponds to weak coupling. The specimens are discretized by a fine mesh of bilinear quadrilateral elements assuming plane stress.

##### 4.1 Four-point shear test

The first example is a four-point shear test of a single-edge-notched beam, conducted by Arrea and Ingraffea (1982), shown in Figure 5. The material parameters chosen are  $E = 30$  GPa,  $\nu = 0.18$ ,  $f_t = 3.5$  MPa and  $G_F = 140$  J/m<sup>2</sup> as used in Patzák and Jirásek (2003). The results are given as contour plots of the maximum principal strain (Figure 6), and load crack mouth sliding displacement (CMSD) curve (Figure 7).

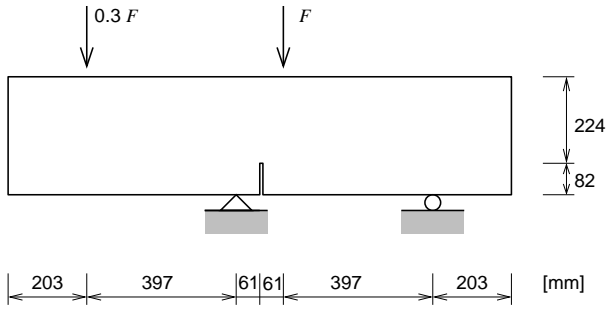


Figure 5: The experimental setup of the four-point shear test.

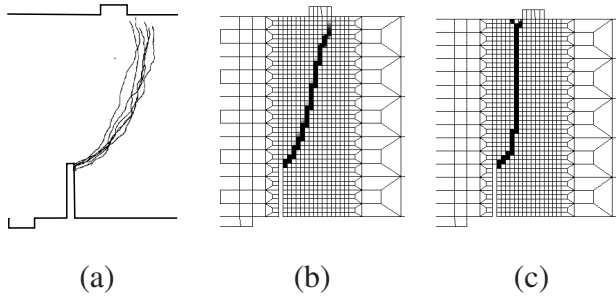


Figure 6: Influence of the volumetric-deviatoric interaction on the crack pattern in the four-point shear test: (a) experiments; (b) strong interaction ( $H_p = 0$ ); (c) weak interaction ( $H_p = 100E$ ).

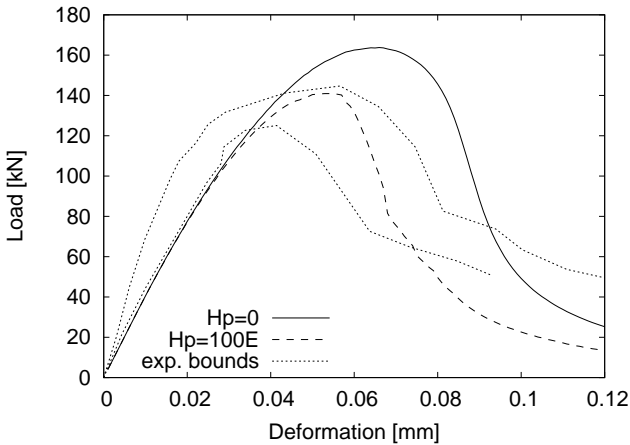


Figure 7: Comparison of load CMSD curves for analysis and experimental bounds in the four-point shear test.

#### 4.2 Double-edge-notched (DEN) specimen

The second example is the double-edge-notched specimen tested by Nooru-Mohamed (1992). The experimental setup is presented in Figure 8.

The non proportional loading path 4c is chosen. This is the most challenging test of the entire program, because the final crack pattern consists of two cracks with a relatively strong curvature, see Figure 9a. During the first stage, the specimen is loaded by an increasing “shear force”,  $P_s$ , until the maximum force that the specimen can carry is reached. Then, in the second stage, this force is kept constant and a “normal” force,  $P$ , is applied in the vertical direction. The material parameters chosen are  $E = 30 \text{ GPa}$ ,  $\nu = 0.2$ ,  $f_t = 3 \text{ MPa}$  and  $G_F = 110 \text{ J/m}^2$  as used in di Prisco et al. (2000) and (Patzák and

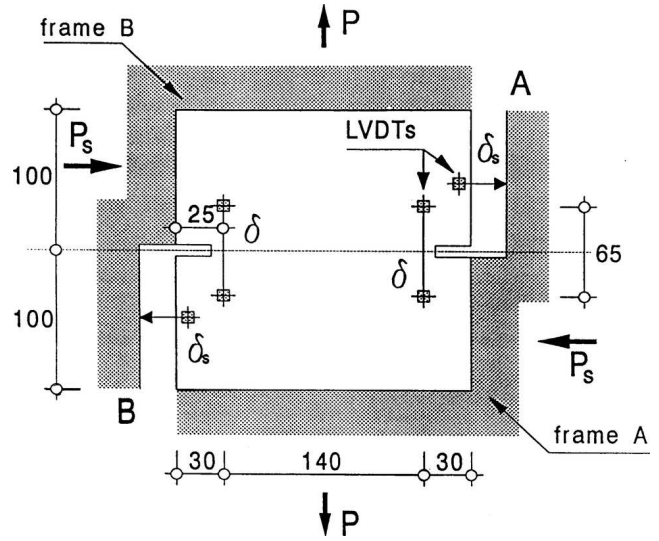


Figure 8: The geometry and the loading setup of the DEN specimen.

Jirásek). The contour plots of the maximum principal strain for strong and weak coupling are compared with the experimental crack patterns in Figure 9. Furthermore, the load-displacement curves for “shear” and “normal” loading are compared with the experimental results in Figure 10, where the simulated load-deflection curve for the normal and shear directions are shown.

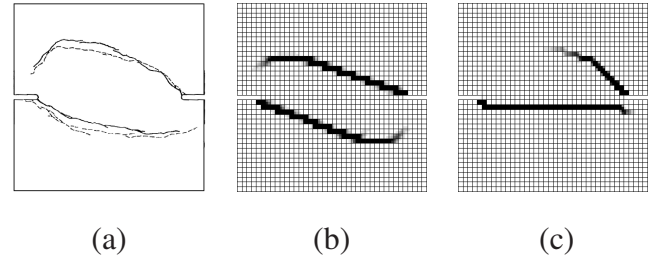
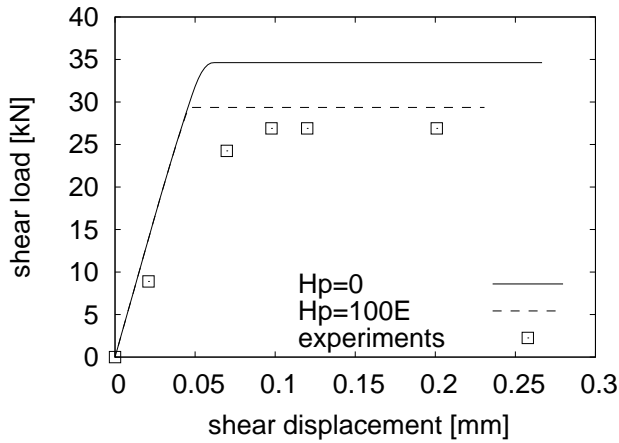


Figure 9: Influence of the volumetric-deviatoric interaction on the crack pattern in the DEN test: (a) experiments, (b) strong interaction ( $H_p = 0$ ), (c) weak interaction ( $H_p = 100E$ ).

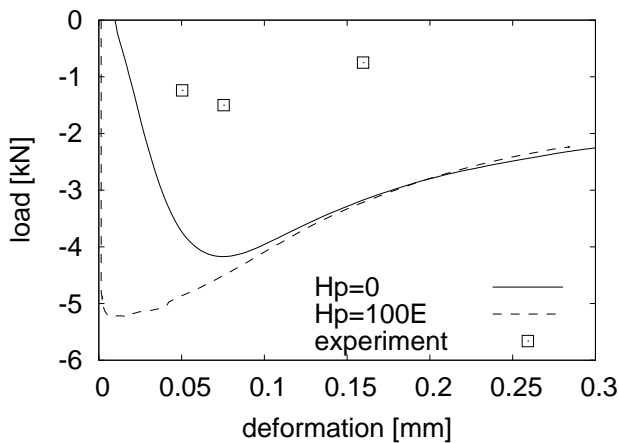
#### 4.3 Discussion of the results

For strong volumetric-deviatoric coupling ( $H_p = 0$ ), the experimental crack patterns are well represented by the elasto-plastic-damage model for both the four-point shear tests and the DEN test, see Figures 6b and 9b. With weak coupling ( $H_p = 100E$ ), on the other hand, the crack patterns cannot be captured. The zone of localized strains in the four-point shear test is strongly attracted by the direction of the mesh lines, see Figure 6c. For the DEN test, the results are even worse. A horizontal localization zone forms as soon as the tensile load is applied in the second stage of the test, see Figure 9c. This does not agree with the curved crack patterns observed in the experiments.

The strain localizes in regions where the stress state is close to uniaxial tension, since zones subjected to shear are confined and resist, therefore, higher



(a)



(b)

Figure 10: Comparison of load-displacement of analysis and experiments of (a) shear force and shear displacement and (b) normal force and normal displacement for the double-edge-notched specimen.

stresses. This is the reason why, for volumetric-deviatoric coupling, the curved crack patterns can be represented, but not without coupling.

## 5 CONCLUSIONS

The study of the influence of volumetric-deviatoric coupling on modeling curved crack patterns leads to the following conclusions.

- Constitutive models with volumetric-deviatoric coupling provide higher shear resistance in simple shear than models without coupling. The increase in shear stress is caused by the activation of compressive stresses due to constrained strains.
- In the simulation of curved cracks, the paths of localized strain zones are strongly influenced by the amount of volumetric-deviatoric coupling. Only with volumetric-deviatoric coupling can the curved crack patterns be reproduced.

Coupling can be provided by the theory of plasticity or anisotropic damage models.

## Acknowledgments

This work was supported by the Swedish Research Council for Environment, Agricultural Sciences and Spatial Planning. The simulations were made using the object-oriented finite element package OOFEM Patzák (1999) and Patzák and Bittnar (2001) extended by the present authors.

## REFERENCES

- Arrea, M. and A. R. Ingraffea (1982). Mixed-mode crack propagation in mortar and concrete. Department of Structural Engineering 81-83, Cornell University, Ithaca, NY.
- Bazant, Z. P. and B.-H. Oh (1983). Crack band theory for fracture of concrete. *Materials and Structures* 16, 155–177.
- Cendón, D. A., J. C. Gálvez, M. Elices, and J. Planas (2000). Modelling the fracture of concrete under mixed loading. *International Journal of Fracture* 103, 293–310.
- di Prisco, M., L. Ferrara, F. Meftah, J. Pamin, R. de Borst, J. Mazars, and J. Reynouard (2000). Mixed mode fracture in plain and reinforced concrete: some results on benchmark tests. *International Journal of Fracture* 103, 127–148.
- Galvez, J. C., M. Elices, G. V. Guinea, and J. Planas (1998). Mixed mode fracture of concrete under proportional and non-proportional loading. *International Journal of Fracture* 94, 267–284.
- Geers, M. G. D., R. de Borst, and R. H. J. Peerlings (2000). Damage and crack modeling in single-edge and double-edge notched concrete beams. *Engineering Fracture Mechanics* 65, 247–261.
- Grassl, P. and M. Jirásek (2004). On mesh bias of local damage models for concrete. In V. Li, C. K. Y. Leung, K. J. Willam, and S. L. Billington (Eds.), *Fracture Mechanics of Concrete Structures*, pp. 323–337.
- Nooru-Mohamed, M. B. (1992). *Mixed-mode fracture of concrete: An experimental approach*. Ph. D. thesis, Delft University of Technology, The Netherlands.
- Ožbolt, J. and H. W. Reinhardt (2002). Numerical study of mixed-mode fracture in concrete. *International Journal of Fracture* 118, 145–161.
- Patzák, B. (1999). Object oriented finite element modeling. *Acta Polytechnica* 39, 99–113.
- Patzák, B. and Z. Bittnar (2001). Design of object oriented finite element code. *Advances in Engineering Software* 32, 759–767.
- Patzák, B. and M. Jirásek (2003). Adaptive resolution of localized damage in quasibrittle materials. *Journal of Engineering Mechanics, ASCE* 130, 720–732.
- Pivonka, P., J. Ožbolt, R. Lackner, and H. A. Mang (2004). Comparative studies of 3d-constitutive models for concrete: application to mixed-mode fracture. *International Journal for Numerical Methods in Engineering* 60, 549–570.
- Schlangen, E. (1993). *Experimental and numerical analysis of fracture processes in concrete*. Ph. D. thesis, Delft University of Technology, Delft, The Netherlands.
- Willam, K., E. Hansen, and H. D. Kang (2001). Performance evaluation of damage and plasticity formulations for concrete. In P. B. Shing and T. Tanabe (Eds.), *Modeling of inelastic behavior of rc structures under seismic load*, pp. 1–19. American Society of Civil Engineers.